bioRxiv preprint doi: https://doi.org/10.1101/090233; this version posted November 29, 2016. The copyright holder for this preprint (which was not certified by peer review) is the author/funder, who has granted bioRxiv a license to display the preprint in perpetuity. It is made available under aCC-BY 4.0 International license.

Title: Structural covariance networks across the lifespan, from 6-94 years of age

Abbreviated Title: Lifespan structural covariance networks

Authors: Elizabeth DuPre & R. Nathan Spreng

Affiliation: Laboratory of Brain and Cognition, Human Neuroscience Institute, Department of Human Development, Cornell University, Ithaca NY, USA

Corresponding Authors:
Elizabeth DuPre
Cornell University
Department of Human Development
Ithaca, NY 14853
emd222@cornell.edu

and

R. Nathan Spreng
Cornell University
Department of Human Development
Ithaca, NY 14853
nathan.spreng@gmail.com

Number of tables: 3
Number of figures: 10
Number of pages: 34
Number of words:
Abstract: 218
Total: 5774; Introduction: 777; Discussion: 1662

Research Highlights

- We examine structural covariance of six neurocognitive networks over the lifespan.
- The structural covariance of these networks exhibits reliable age-dependent trends.
- Hub regions significantly influence trajectories of structural covariance.
- Structural covariance appears to partially reflect a shared functional history.

bioRxiv preprint doi: https://doi.org/10.1101/090233; this version posted November 29, 2016. The copyright holder for this preprint (which was not certified by peer review) is the author/funder, who has granted bioRxiv a license to display the preprint in perpetuity. It is made available under aCC-BY 4.0 International license.

Abstract

Structural covariance examines interindividual differences in the covariation of grey matter morphology between brain regions. Although structural covariance has been used to examine the development of brain networks in either adolescence or aging, no study to date has provided a lifespan perspective on the development of structural covariance networks, bridging childhood with early and late adulthood. Here, we investigate the lifespan trajectories of structural covariance in six canonical neurocognitive networks default, dorsal attention, frontoparietal control, somatomotor, ventral attention, and visual networks. By combining data from five open access data sources, we examine the structural covariance trajectories of these networks from 6-94 years of age in a sample of 1580 participants. Using partial least squares, we show that structural covariance patterns across the lifespan exhibit two significant, age-dependent trends. The first trend is a rapid decline that levels off in later life, suggestive of reduced within-network covariance. The second trend is an inverted-U that peaks in young adulthood, suggestive of the patterns of integration followed by de-differentiation as observed in functional brain networks. Hub regions, including posterior cingulate cortex and anterior insula, appear particularly influential in the expression of this second age-dependent trend. Overall, we suggest that these results provide evidence for the importance of a persistent pattern of functional coupling in the developmental trajectories of structural covariance networks.

Keywords: Network, structural covariance, grey matter, development, aging, MRI

bioRxiv preprint doi: https://doi.org/10.1101/090233; this version posted November 29, 2016. The copyright holder for this preprint (which was not certified by peer review) is the author/funder, who has granted bioRxiv a license to display the preprint in perpetuity. It is made available under aCC-BY 4.0 International license.

1. Introduction

The human cerebral cortex is hierarchically organized into complex brain networks that can be considered at multiple levels of analysis (Mesulam, 1998). One such level is structural covariance, or how interindividual differences in regional brain structure covary with other brain structures across the population (Mechelli, Friston, Frackowiak, & Price, 2005; Alexander-Bloch, Giedd, & Bullmore, 2013). Structural covariance networks reflect shared variation in grey matter morphology (Mechelli et al., 2005) and are assessed using measures such as cortical thickness and regional volume. These networks exhibit reproducible organization at both a population (Alexander-Bloch et al., 2013) and individual (Tijms, Seris, Willshaw, & Lawrie, 2012) level and have been identified across species (Pagani, Bifone, & Gozzi, 2016), underscoring their role as an intrinsic feature of cortical organization.

The organization of grey matter morphology into structural covariance networks mirrors the organization of intrinsic brain activity into large-scale functional networks (Bullmore & Sporns, 2009). Large-scale functional networks have been reliably identified using resting-state functional connectivity (Yeo et al., 2011; Power et al., 2011) and linked to cognition and behavior (Stevens & Spreng, 2014). There is an increasing understanding of the relationship between large-scale functional networks and anatomical connectivity (Mišić et al., 2016), with a many-to-one mapping between diverse functional activity patterns and underlying anatomical connections. However, there is significantly less understanding of the relationship between large-scale functional and structural covariance networks, and the appropriate technique to assess such a relationship is still an active area of investigation (Geerligs, Cam-CAN, & Henson, 2016). Despite uncertainty around the relationship between large-scale functional and structural systems, grey matter organization at an areal level has been shown to significantly impact functional activity and connectivity (Sui, Huster, Yu, Segall, Calhoun, 2014), underscoring the existence of a structural scaffold for functional activation (Bullmore & Sporns, 2009).

The source of grey matter shared covariance patterns is unclear and has been hypothesized to reflect both genetic and plastic influences including maturational timing (Alexander-Bloch, Raznahan, Bullmore, & Giedd, 2013). Indeed, age is a significant moderator of functional (Dosenbach et al., 2010; Chan, Park, Savalia, Petersen, & Wig, 2014) and anatomical (Collin & van den Heuvel, 2013; Hagmann et al., 2010) connectivity. Some of the most extensive age effects occur in grey matter (Giorgio et al., 2010). Grey matter organization undergoes significant structural change with age including synaptic proliferation, pruning, and eventual atrophy (Low & Cheng, 2006; Fjell et al., 2010). In structural covariance networks, these changes are seen as increasing long-range covariance across early development (Zielinski, Gennatas, Zhou, & Seeley, 2010) before shifting to increased local covariance with advancing age (Montembeault et al., 2012). Normative grey matter changes do not occur simultaneously and show variation across cortex (Krongold, Cooper, & Bray, 2015; Raz et al., 2005), and this is

bioRxiv preprint doi: https://doi.org/10.1101/090233; this version posted November 29, 2016. The copyright holder for this preprint (which was not certified by peer review) is the author/funder, who has granted bioRxiv a license to display the preprint in perpetuity. It is made available under aCC-BY 4.0 International license.

reflected in substantial variation of structural covariance network trajectories. Networks containing sensorimotor structures, for example, show relatively preserved organization in aging (Hafkemeijer et al., 2014). Importantly, existing studies examine the trajectories of structural covariance networks in isolated developmental epochs (e.g., child development, advanced age), which may limit our understanding of the normative life cycle of each of these networks.

Despite significant progress in understanding structural covariance at both ends of the lifespan, to date no study has examined the development of large-scale structural covariance networks across the entire lifespan. This is in contrast to continued interest in the trajectory of large-scale functional networks across the lifespan (Zuo et al., 2016), where functional networks have been shown to undergo significant reorganization with age. The changes seen in the developmental trajectory of large-scale functional networks suggest that a lifespan study of structural covariance networks will provide an important complement, yielding insights into cortical organization at the level of grey matter morphology.

In this study, our primary aim was to provide comprehensive mapping of the neurocognitive large-scale structural covariance networks across the entire lifespan. We collapsed data across five publicly available datasets to provide a normative sample ranging from six to ninety-four years of age. This also afforded us sufficient power for reliable estimates of structural covariance networks at six developmental epochs: childhood (6-15y), adolescence (16-25y), young adulthood (26-35y), middle adulthood (36-59y), late adulthood (60-75y), and older adulthood (76-94y). We assessed the structural covariance of six large-scale brain networks well represented in the literature: The default network (DN), dorsal attention network (DAN), frontoparietal control network (FPCN), somatomotor network (SM), ventral attention network (VAN), and visual systems (c.f. Yeo et al., 2011). Whole-brain structural covariance was assessed in a seed-based multivariate analysis (Spreng & Turner, 2013; Persson et al., 2014). We examined both shared and unique lifespan developmental trajectories across networks, and what these changes might reveal about the developmental organization of neurocognitive grey matter networks.

2. Materials and Methods

2.1. Image Acquisition

Data were collated from five open access data sources: National Institutes of Health Pediatric MRI Data Repository (NIH-Peds; Brain Development Cooperative Group & Evans, 2007): Release 5, Human Connectome Project (HCP): 500 subjects release, Nathan Kline Institute-Rockland Sample (NKI-RS; Nooner et al., 2012): Release 5, Open Access Series of Imaging Studies (OASIS), and Alzheimer's Disease Neuroimaging Initiative (ADNI). A complete listing of T1-weighted anatomical image acquisition procedures for each data source is provided in Table 1.

bioRxiv preprint doi: https://doi.org/10.1101/090233; this version posted November 29, 2016. The copyright holder for this preprint (which was not certified by peer review) is the author/funder, who has granted bioRxiv a license to display the preprint in perpetuity. It is made available under aCC-BY 4.0 International license.

2.2. Participant Characteristics

From each sample, only healthy control participants greater than six years of age with no diagnosed history of DSM Axis I or II disorder were considered. Six years was chosen as the lowest estimate for lifespan characterization, since previous work has indicated that normalization for children less than six years is likely to introduce significant artifacts (Muzik, Chugani, Juhász, Shen, & Chugani, 2000) as grey matter volume in younger children is less than 95% of that observed in adults (Caviness, Kennedy, Richelme, Rademacher, & Filipek, 1996). For individuals meeting these criteria, the T1-weighted anatomical image was selected. In the case of longitudinal data, only the first time point was selected for each participant.

All T1-weighted anatomical images (n = 1667) were visually inspected for quality assurance: images that showed evidence of artifacts were excluded (n = 87), yielding a final sample size of n = 1580 (age *M* = 35y, *SD* = 23y, Range = 6 - 94y; 659 males; 859 scanned at 1.5T and 721 at 3T). Participants were then sorted into the following age groups: childhood (6-15y), adolescence (16-25y), young adulthood (26-35y), middle adulthood (36-59y), late adulthood (60-75y), and older adulthood (76-94y). See Table 2 for sample sizes and participant characteristics by age group.

Although we sought to create cohorts representing neurobiologically meaningful age ranges, this resulted in unequal representation for some ranges of the lifespan. In particular, middle adulthood, defined here as ages 36-59, spans a larger time period than any of the other cohorts considered. This was in large part due to the paucity of openly available data for that cohort, particularly when compared to other cohorts such as younger adulthood. As so little work has investigated the functional and structural changes that occur in this age range, we have little evidence that our definition of middle adulthood negatively impacts the present work, or that this age range should be additionally subsampled into smaller, neurobiologically representative cohorts. Nonetheless, future work utilizing cross-sectional data for lifespan investigations should aim to include more subjects in this under-sampled age range. The continuing collection of multi-modal data for lifespan initiatives such as NKI-RS (Nooner et al., 2012) and the HCP Lifespan Project (Glasser et al., 2016) will increase the availability of high-quality data to investigate such questions.

2.3. Segmentation and Preprocessing

Each age group was separately submitted to voxel-based morphometry (Ashburner & Friston, 2000) using the VBM8 toolbox (www.neuro.uni-jena.de/vbm/) implemented in Matlab (MATLAB 8.0, MathWorks, Natick, MA, 2012). Images were first segmented into grey matter, white matter, and cerebrospinal fluid using an extension of the New Segmentation algorithm. Grey matter images for this age group were then affine registered to the MNI template and carried to the Diffeomorphic Anatomical Registration through Exponentiated Lie Algebra toolbox (DARTEL; Ashburner, 2007)

bioRxiv preprint doi: https://doi.org/10.1101/090233; this version posted November 29, 2016. The copyright holder for this preprint (which was not certified by peer review) is the author/funder, who has granted bioRxiv a license to display the preprint in perpetuity. It is made available under aCC-BY 4.0 International license.

where they were iteratively aligned to create an age-group-specific template in MNI space.

As discussed below, two additional analyses exploring network definition and overlap with functional definitions were conducted using only the young adulthood cohort (26-35y); for these analyses, the young adult images were aligned to their age-group-specific template in MNI space. For all other analyses, the six resulting age-group-specific templates were themselves then iteratively aligned again using DARTEL to create a study-specific template in MNI space. Importantly, this study-specific template equally weighted each of the age ranges represented by the six age groups.

Finally, previously segmented images were aligned to the study-specific template of interest using DARTEL high-dimensional normalization within VBM8. Non-linear only modulation was applied to grey matter images to derive regional differences in grey matter volume, correcting for head size. Modulated grey matter images were iteratively smoothed to 8mm FWHM using *3dBlurToFWHM* in AFNI (Cox, 1996) and carried forward for further analysis.

2.4. Network Identification

In this study, we sought to examine the structural covariance of the large-scale neurocognitive networks, including the DN, DAN, FPCN, SM, VAN, and visual networks. To examine each of these six networks, grey matter volumes for four selected high-confidence seeds reported in Yeo et al. (2011) were extracted. A listing of all 24 seeds and their network affiliations is presented in Table 3, and a visual representation of their location on cortex is presented in Figure 1. Extracted grey matter volumes were then averaged across the four seeds for each participant.

We first conducted an analysis to confirm that the network definition obtained by averaging the four seeds provided more selective, network-specific spatial patterns than either one of the seeds individually or including all four seeds as separate vectors. We then conducted a second analysis to examine the overlap of structural covariance network definitions with functional characterizations, and the specificity of structural covariance to the neurocognitive network of interest. For these two analyses, only anatomical images from the young adult cohort (26-35y), aligned to the young adult template in MNI space, were used. For the network definition analysis, the DN was chosen as an exemplar network to explore the impact of seed averaging, resulting in four 472 × 1 vectors and one 472 × 4 matrix. To foreshadow the results, averaging the seeds provided reliable, network specific maps. For the functional overlap analysis, then, all six neurocognitive networks were examined by averaging the extracted grey matter volumes for each of the network-specific seeds, resulting in six 472 × 1 vectors.

For analyses using the full age range of 6-94 years, all six neurocognitive networks were examined by averaging the extracted grey matter volumes for each of the network-specific seeds, resulting in a 1580 × 1 vector for each network. For each of the analyses, this vector **Y** represented the average grey matter volume for each participant of

bioRxiv preprint doi: https://doi.org/10.1101/090233; this version posted November 29, 2016. The copyright holder for this preprint (which was not certified by peer review) is the author/funder, who has granted bioRxiv a license to display the preprint in perpetuity. It is made available under aCC-BY 4.0 International license.

key nodes within the network. The resulting vectors and matrices were submitted to Partial Least Squares (PLS; McIntosh, Bookstein, Haxby, & Grady, 1996).

2.5. Partial Least Squares (PLS) Analyses

PLS is a data-driven multivariate statistical technique capable of identifying patterns of structural covariance (Spreng & Turner, 2013; Persson et al., 2014). We utilized seed PLS to identify patterns of covariance between grey material integrity in seed regions and whole brain structural MRI images (for a review, see Krishnan, Williams, McIntosh, & Abdi, 2011).

2.5.1. Derivation of Covariance Matrix

For experimental analyses, our seed value was the average grey matter volume of four selected high-confidence seeds reported in Yeo et al. (2011). The vector **Y** representing this average grey matter volume was cross-correlated with a matrix **X** of participant's structural images. Importantly, this participant image matrix contained six sub-matrices $\mathbf{X}_{1..6}$ corresponding to each age group. We retained this age group organization in our PLS analyses in order to directly compare age groups in their structural covariance between average network and whole brain grey matter volume. Both the grey matter volume vector and image matrix were centered and normalized within age groups such that their cross-correlation resulted in a covariance matrix **Z** according to:

$$\boldsymbol{Y}^{\boldsymbol{T}}\boldsymbol{X} = \boldsymbol{Z} \tag{1}$$

Note that this covariance matrix is equivalent to a correlation matrix due to the described within-group normalization. The resulting covariance matrix **Z** measures the degree to which the network average and whole brain grey matter volumes co-vary at a voxel-wise level for each participant.

2.5.2. Singular Value Decomposition

Using singular value decomposition (SVD; Eckart & Young, 1936), the covariance matrix **Z** from Eq. (1) was then decomposed into:

$$\boldsymbol{Z} = \boldsymbol{U}\boldsymbol{\Delta}\boldsymbol{V}^{\boldsymbol{T}} \tag{2}$$

where **V** is the matrix of right singular vectors, **U** is the matrix of left singular vectors, and **Δ** is the diagonal matrix of singular values. The right and left singular vectors represent the grey matter seed integrity profiles and spatial patterns that best characterize the covariance matrix **Z**. The triplet of the right and left singular vectors and the singular values forms a set of mutually orthogonal Latent Variables (LVs) where the number of LVs derived is equal to the rank of the covariance matrix **Z**. In our analyses, this identified six LVs for each network corresponding to the six sub-matrices of **Z**. Each LV was tested for statistical significance with 5000 permutations and cross-validated for reliability with 1000 bootstraps. Bootstrap ratios, derived from dividing the weight of the singular-vector by the bootstrapped standard error, are equivalent to z-scores and were used to threshold significant LV spatial patterns at a 95% confidence interval for projection and interpretation.

bioRxiv preprint doi: https://doi.org/10.1101/090233; this version posted November 29, 2016. The copyright holder for this preprint (which was not certified by peer review) is the author/funder, who has granted bioRxiv a license to display the preprint in perpetuity. It is made available under aCC-BY 4.0 International license.

Patterns were considered for further analysis based on two criteria. First, latent variables (LVs) must be statistically significant by permutation testing at the level of $p < 0.001$. Second, LVs must account for a minimum of 5% of the covariance in the data.

For the network definition and functional overlap analyses, the covariance matrix and resulting singular value decomposition were performed equivalently, with the exception that there were no sub-matrices in the covariance matrix, as only young adult participants (26-35y) were included.

2.5.3. Derivation of Subject Scores

We also quantified individual contributions to each LV by deriving subject scores. Of particular interest in this work are the subject scores known in PLS nomenclature as "brain scores," which assess the contribution of each individual to the group structural covariance pattern. Multiplying the original matrix **X** of participant structural images by the matrix of right singular vectors **V** derive these brain scores as follows:

$$\boldsymbol{L} = \boldsymbol{XV} \tag{3}$$

where **L** is a matrix of brain scores. Recall from Eq. (2) that the right singular vector **V** represents the seed-integrity profiles that best characterizes the covariance matrix **Z**, such that multiplying this singular vector by the participant structural images derives the seed integrity profiles for each participant that reflect their contribution to the group structural covariance pattern. The matrix of brain scores **L** was extracted for each LV where, for each participant, this brain score value represents a weighted value of grey matter integrity within the regions identified in the group image. To account for potential confounds, we ran a multiple regression of these brain scores against scanner strength and gender. Residuals from this regression were plotted against age to visualize the covariance of the associated spatial pattern across the population.

3. Results

We investigated the structural covariance of previously identified large-scale neurocognitive networks including the DN, DAN, FPCN, SM, VAN, and visual networks. Using Partial Least Squares (PLS), we identified patterns of structural covariance for each of the six networks examined.

3.1 Seed Averaging in Neurocognitive Network Definition

We first conducted an analysis to examine the impact of seed averaging on network definition. We restricted this analysis to the DN in the young adult (26-35y) cohort to minimize age- and network-specific effects. Results are presented in Figure 2 with DN resting-state functional connectivity boundaries as defined by Yeo and colleagues (2011) overlaid in red. As seen in Figure 2A-2D, using individual seeds for network definition results in structural covariance patterns that are either localized to the seed region or fail to extend to the contralateral hemisphere. Using all four seeds for network definition, without averaging, results in a structural covariance pattern presented

bioRxiv preprint doi: https://doi.org/10.1101/090233; this version posted November 29, 2016. The copyright holder for this preprint (which was not certified by peer review) is the author/funder, who has granted bioRxiv a license to display the preprint in perpetuity. It is made available under aCC-BY 4.0 International license.

in Figure 2E that includes canonical network regions, but also includes non-network-specific features. Figure 3A shows the resultant structural covariance pattern when using the averaged, extracted grey matter volume of all four seed regions. The resulting spatial pattern provides the most robust network characterization that retains selectivity for network-specific features. Based on these results, we chose to utilize averaged seed vectors for all following analyses.

3.2 Network Definition Assessed against Functional Characterization

We conducted a second analysis to directly examine the overlap between neurocognitive network structural covariance and functional characterizations, defined by resting-state functional connectivity boundaries. This analysis was performed only in the young adult cohort (26-35y) to enhance comparisons with results provided by Yeo and colleagues (2011). For each of the six neurocognitive networks, results are presented in Figure 3 and overlaid with resting-state functional connectivity boundaries as defined by Yeo and colleagues (2011). Visual inspection suggests that there is low to moderate overlap between network structural covariance definition and functional characterization.

To quantitatively assess overlap, we calculated the Dice similarity coefficient between the structural covariance pattern and the resting-state functional connectivity definition for each network. A heat map depicting the full matrix of Dice coefficients comparing each structural covariance spatial pattern to resting-state functional definitions of the six neurocognitive networks is presented in Figure 4. In general, structural covariance network definitions show low overlap with their functional characterizations, with Dice coefficients averaging 0.14 (Range: 0.08-0.21). With the exception of the SM, however, all structural covariance networks show the highest similarity with their respective functional parcellation. The structural covariance pattern of SM does show slightly higher similarity for the resting-state functional connectivity parcellation of VAN (0.11 for SM; 0.12 for VAN). This heightened similarity may be due to strong structural covariance of insular cortex, a known somatomotor structure and functionally fine-grained region (Chang, Yarkoni, Khaw, & Sanfey, 2013), with VAN.

3.3 Neurocognitive Network Structural Covariance Patterns

PLS analyses of each of the large-scale networks examined yielded multiple significant LVs, corresponding to reliable patterns of structural covariance within each network. We review significant results for each of the networks in turn.

3.3.1. Default Network

Two significant LVs were identified for the DN and are presented in Figure 5. In the first LV ($p < 0.0002$), seeded regions, along with homologous contralateral regions, covary together as well as with parahippocampal cortex and lateral temporal cortex (Fig 5A). Covariance extended to non-canonical DN regions including posterior insula. All age groups showed a robust positive association with this pattern (Figure 5B); this suggests that this latent variable corresponds to the structural covariance of the DN as it is preserved across the lifespan. Extracted brain scores (Fig 5C) revealed that the integrity

bioRxiv preprint doi: https://doi.org/10.1101/090233; this version posted November 29, 2016. The copyright holder for this preprint (which was not certified by peer review) is the author/funder, who has granted bioRxiv a license to display the preprint in perpetuity. It is made available under aCC-BY 4.0 International license.

of this structural covariance pattern declines with advancing age, at first rapidly before reaching a plateau at approximately 70 years of age.

The second significant LV ($p < 0.0002$) showed structural covariance patterns of developmental change in the DN. Adolescents (16-25y) showed a unique pattern of increased structural covariance with medial prefrontal cortex and anterior insula compared to all other age groups examined (Figure 5D, E). Age groups with reliable averaged subject scores—those for which the confidence interval did not cross zero—included the childhood (6-15y), young adulthood (26-35y), late adulthood (60-75y), and older adulthood (76-94y) cohorts. Compared to adolescence (16-25y), each of these cohorts showed relatively increased structural covariance between seeded DN regions and sensorimotor structures including motor and visual cortices as well as thalamus. Across the lifespan, this pattern shows a nearly linear decrease with advancing age (Figure 5F), suggesting that older adults are less strongly aligning to the structural covariance pattern depicted in Figure 5D.

3.3.2. Dorsal Attention Network

Two significant LVs were identified for the DAN and are presented in Figure 6. In line with results presented for the DN, the first significant DAN LV ($p < 0.0002$) showed seeded regions positively covarying together as well as with canonical DAN regions such as intaparietal sulcus (Figure 6A). Covariance also extended to other, non-canonical DAN regions, including posterior insula and subgenual cingulate. All age groups showed a robust association with this pattern (Figure 6B). Brain scores reveal that the integrity of this pattern shows rapid decline with advancing age before plateauing at approximately 70 years (Figure 6C).

The second significant LV ($p < 0.0002$) revealed developmental changes in the structural covariance pattern of the DAN. Adolescents (16-25y) showed uniquely increased structural covariance with medial prefrontal cortex and anterior insula. Older age groups show relatively increased structural covariance between the seeded DAN regions and areas including motor and visual cortices as well as subcortical structures. Inspection of brain scores (Figure 6F) reveals an inverted U-shaped trajectory, with integrity of the structural covariance pattern reaching its peak in young adulthood, while very young and very old individuals show significantly less integrity for the derived group structural covariance patterns.

3.3.3. Frontoparietal Control Network

Two significant LVs were identified for the FPCN and are depicted in Figure 7. Similar to results seen for the DN and DAN, the first significant LV ($p < 0.0002$) showed a structural covariance pattern that was positively associated with all examined age groups, but showed a non-linear decline in integrity across the lifespan. Seeded FPCN regions positively covary together, as well as with structures consistently associated with cognitive control, such as lateral prefrontal cortex, and non-canonical FPCN regions, such as posterior insula.

bioRxiv preprint doi: https://doi.org/10.1101/090233; this version posted November 29, 2016. The copyright holder for this preprint (which was not certified by peer review) is the author/funder, who has granted bioRxiv a license to display the preprint in perpetuity. It is made available under aCC-BY 4.0 International license.

The second LV ($p < 0.0002$) revealed developmental trajectories of structural covariance patterns in the FPCN. There was a significant dissociation between children and adolescents (6-25y) as compared to middle and late adulthood (36-75y). Younger age groups show increased structural covariance with structures both within the canonical FPCN such as precuneus as well as with non-canonical regions such as lateral temporal cortex. Older age groups, however, show relatively increased structural covariance for sensorimotor structures such as motor cortex and thalamus. Brain scores suggest an inverted U-shaped trajectory similar to that seen for the DAN, with the integrity of the structural covariance pattern at its highest levels in young adulthood.

3.3.4. Somatomotor Network

Two significant LVs were identified for the SM and are depicted in Figure 8. In agreement with the previously reported networks, the first significant LV ($p < 0.0002$) showed a structural covariance pattern that is positively associated with all examined age groups and shows a non-linear decline with advancing age. Seeded regions covaried together as well as with the motor strip. Covariance extended to areas outside the canonical motor network such as lateral prefrontal cortex and subcortical regions.

The second LV ($p < 0.0002$) showed a significant dissociation between children and adolescents (6-25y) as compared to middle, late, and older adulthood (36-94y). Younger age groups show increased structural covariance with structures outside of the canonical motor network such as lateral temporal cortex and mid-insula, while older age groups show relatively increased structural covariance local to the seed regions and to thalamus. Similar to the individual subject score trajectories seen for the DAN and FPCN, there is an inverted U-shaped trajectory in the integrity of this structural covariance pattern, with integrity reaching a peak in young adulthood before beginning to decline.

3.3.5. Ventral Attention Network

Two significant LVs were identified for the VAN and are presented in Figure 9. The first LV ($p < 0.0002$) again shows a structural covariance pattern positively associated with all examined age groups. Seeded VAN regions positively covary together and with the mid- and posterior insula as well as with the medial prefrontal cortex. Extracted brain scores revealed a non-linear decline in the integrity of this structural covariance pattern across the lifespan.

The second significant LV ($p < 0.0002$) revealed a pattern of developmental change similar to that seen in DN, with individuals in adolescence (16-25y) and middle adulthood (36-59y) showing a unique structural covariance pattern compared to all other age groups. Specifically, these two groups showed increased structural covariance with medial prefrontal as well as parahippocampal cortex. Other age groups showed increased structural covariance with sensorimotor structures such as motor and visual cortices. Similarly to the DN, there is a near linear decrease in structural integrity across the

bioRxiv preprint doi: https://doi.org/10.1101/090233; this version posted November 29, 2016. The copyright holder for this preprint (which was not certified by peer review) is the author/funder, who has granted bioRxiv a license to display the preprint in perpetuity. It is made available under aCC-BY 4.0 International license.

lifespan, with older adults showing decreased structural covariance between seeded VAN regions and sensorimotor structures.

3.3.6. Visual Network

One significant LV ($p < 0.0002$) was identified for the visual network and is presented in Figure 10. As in previous networks, the significant LV revealed a structural covariance pattern that was positively associated with all examined age groups and non-linearly declined with age. Seeded visual regions showed positive structural covariance with visual cortex as well as with non-canonical visual regions such as the posterior insula and mid-cingulate.

4. Discussion

In this study, we examined developmental trajectories of structural covariance in large-scale neurocognitive networks across the lifespan using publicly available cross-sectional data. Structural covariance networks show two broad developmental patterns: a stable pattern that reflects the structural configuration of the network and persists across the lifespan, and an age-dependent pattern that reveals common age-related trajectories of structural covariance across networks.

Across all networks, the first significant latent variable—accounting for the majority of the explained covariance—identified a structural covariance pattern whose spatial extent was unique to the neurocognitive network of interest and persisted across all age groups examined. Plotting individual subject scores or "brain scores" for these latent variables as in panel C of Figures 5-10 revealed a rapid decline in grey matter network integrity with advancing age, followed by a plateau at approximately 70 years.

With the exception of the visual network, all networks additionally showed a second significant latent variable with differential expression over the life course. Examination of brain scores seen in panel F of Figures 5-9 reveals that these could be broadly considered as aligning with an inverted U-shaped trajectory, particularly for the DAN, FPCN, and SM. In addition to the trajectory seen in these brain scores, these latent variables also showed unique spatial features of positive and negative structural covariance at a group level, shown in panel D of Figures 5-9. On either end of the lifespan, neurocognitive networks showed positive structural covariance of the seeded regions with sensorimotor structures including motor and visual cortices as well as thalamus. A reliably different pattern of structural covariance was seen in adolescence, with positive structural covariance between the seeded regions and structures including medial prefrontal cortex, posterior cingulate, insular cortex, and temporal cortex.

The second significant variables of the DN and VAN show these shared spatial features of positive and negative structural covariance; however, the trajectories seen in panel F of Figures 5 and 9 do not show a reliable, inverted U-shape. Instead, the second latent variable of these networks appears to exhibit a near linear decline across the lifespan. One possible explanation for this difference is that the selected seed regions for

bioRxiv preprint doi: https://doi.org/10.1101/090233; this version posted November 29, 2016. The copyright holder for this preprint (which was not certified by peer review) is the author/funder, who has granted bioRxiv a license to display the preprint in perpetuity. It is made available under aCC-BY 4.0 International license.

the DN and VAN included regions such as the medial prefrontal cortex, posterior cingulate, and insular cortex. These regions are known functional hubs (van den Heuvel & Sporns, 2013); and in the second latent variable of DAN, FPCN, and SM, their structural covariance reliably differentiates adolescence from other portions of the lifespan. In PLS, successive latent variables contribute unique, additional portions of the variance. Since these seed regions strongly contribute to the structural covariance of the DN and VAN first latent variables, it is possible that the appearance of a near linear decline in the second latent variable—rather than an inverted U-shaped trajectory—is due to the exclusion of medial prefrontal cortex, posterior cingulate, and insular cortex from the second latent variables of the DN and VAN. This would suggest that these regions are particularly important in shaping age-dependent patterns of structural covariance.

Our results therefore suggest that the structural covariance patterns of large-scale neurocognitive networks each have a unique spatial topology; however, networks also show overlapping patterns of age-dependent structural covariance.

4.1 Persistent Patterns of Structural Covariance

For each of the neurocognitive networks examined, a significant latent variable was identified revealing network-specific, stable patterns of structural covariance that persisted across all age groups. Despite the stability of these structural covariance patterns across age groups, inspection of individual subject or "brain" scores revealed that integrity to these patterns declines rapidly with advancing age before plateauing at approximately 70 years. It is possible that these declines in individual subject integrity emerge in interaction with changes in within-network functional connectivity, which has also been shown to decrease with age (Betzel et al., 2014).

The structural covariance patterns identified for each neurocognitive network did not show strong overlap with their functional definitions. Calculating the Dice coefficient for network definition in young adulthood revealed approximately 20% overlap between structural covariance and functional network boundaries. In general, structural covariance networks showed spatial patterns that recall sparse network-specific functional connectivity; however, they also showed non-canonical features. For example, the DN showed positive structural covariance between the seeded regions and the anterior insula, a hub region canonically associated with the ventral attention network (Craig, 2009). The default and ventral attention networks show strong functional interactions (Jilka et al., 2014), suggesting that structural covariance patterns may partially reflect persistent pattern of functional coupling across the lifespan.

4.2 Age-Dependent Patterns of Structural Covariance

In addition to stable patterns of structural covariance, all networks examined except the visual network showed an additional, age-dependent pattern that differentiated young adulthood from either end of the lifespan. In young adulthood, seeded regions showed positive structural covariance with a set of regions including medial prefrontal cortex, posterior cingulate, insular cortex, and temporal cortex— association cortices

bioRxiv preprint doi: https://doi.org/10.1101/090233; this version posted November 29, 2016. The copyright holder for this preprint (which was not certified by peer review) is the author/funder, who has granted bioRxiv a license to display the preprint in perpetuity. It is made available under aCC-BY 4.0 International license.

corresponding to known functional hubs (van den Heuvel & Sporns, 2013). In both childhood and older adulthood, however, seeded regions showed positive structural covariance with sensorimotor structures including motor and visual cortices as well as thalamus.

These results mirror developmental trajectories commonly reported in functional connectivity studies with increased functional integration across networks in childhood, peak functional segregation between networks in young adulthood, and de-differentiation of network functional connectivity in older adulthood (Collin & van den Heuvel, 2013). The structural covariance patterns reported here suggest that, during peak functional segregation in young adulthood, networks show increased structural covariance with hub regions as they facilitate information flow across networks. In both childhood and older adulthood, networks show increased structural covariance with sensorimotor structures mirroring their high functional degree in early development (Collin & van den Heuvel, 2013) and relatively preserved functional connectivity in aging (Geerligs, Renken, Saliasi, Maurits, & Lorist, 2015). Inspection of brain scores confirmed this pattern, revealing an inverted U-shaped trajectory that peaked in young adulthood. The visual network did not have a second, significant latent variable, suggesting that this network does not show the same age-dependent patterns of structural covariance as other networks. This could be due to the relative preservation of within-network connectivity in the visual system compared to other networks (Chan et al., 2014).

4.3 Relationship of Structural Covariance to Function

Structural covariance networks have been extensively linked to neural function via their marked disruptions in pathology and pathological aging (Bassett et al., 2008; Hafkemeijer et al., 2016; Spreng & Turner, 2013; Valk, Martino, Milham, & Bernhardt, 2015). Alongside functional connectivity, shared structural covariance has been suggested as a defining characteristic of large-scale networks (Seeley, Crawford, Zhou, Miller, & Grecius, 2009). Although the results presented here suggest that there is little overlap in network definitions by structural covariance as compared to functional connectivity, they nonetheless suggest a bridge between structural covariance and network function. In particular, the strong overlap of age-dependent structural covariance trajectories with those reported in the functional connectivity literature may in part explain the noted relationship between structural covariance and neural function.

4.4. Methodological Considerations

Although this study was uniquely able to leverage the increasing amount of anatomical data available in open-access repositories, usage of the selected data sources introduced several important methodological considerations related to scanner acquisition strength and motion correction. The first set of limitations concerns the differential acquisition strength at which anatomical scans were acquired across studies. Several data sources, including those representing the youngest and oldest subjects, were acquired at 1.5T, while anatomical scans of young adults were acquired at 3T. Although it is likely

bioRxiv preprint doi: https://doi.org/10.1101/090233; this version posted November 29, 2016. The copyright holder for this preprint (which was not certified by peer review) is the author/funder, who has granted bioRxiv a license to display the preprint in perpetuity. It is made available under aCC-BY 4.0 International license.

that subtle differences between groups may have been introduced by MR field strength rather than true age-specific differences, we do not believe that these effects drive our current results. To confirm this, we also included two additional, lifespan data sources of 1.5T and 3T field strength (OASIS and NKI-RS, respectively), which do not show divergent results from those seen in the age-restricted datasets. We additionally assessed the impact of controlling for MR field strength in our individual subject or "brain" scores and found similar results for both raw and corrected subject scores. Although we do not believe that differential field strength across studies negatively impacted the current study, future work assessing structural covariance across the lifespan should aim to examine scans acquired at the same MR field strength and ideally on the same scanner. Recent initiatives such as the UK Biobank (Miller et al., 2016) promise the availability of large, high-quality datasets for such investigations.

An additional limitation of the current study is the inability to implement motion correction of structural images. Recent work has shown that head motion may introduce artifacts into anatomical images, affecting automated estimates of structure such as voxel-based morphometry and cortical thickness (Alexander-Bloch et al., 2016; Savalia et al., 2016). Although acquisition of a resting-state scan has been proposed to estimate stable inter-individual differences in motion and flag high-motion subjects for exclusion from structural analyses (Alexander-Bloch et al., 2016; Savalia et al., 2016), not all of the datasets utilized also provided at least one resting-state scan for each subject. We therefore caution that estimates of age-group differences may be inflated by uncorrected motion and urge future work to investigate the age-related trajectory of structural covariance patterns in motion-corrected data.

Each of these methodological considerations can be addressed in future work, as comprehensive samples of participants across the lifespan with both structural and functional imaging become increasingly available.

5. Conclusions

In this study we utilized open-access, cross-sectional data sources to examine structural covariance patterns of six neurocognitive networks across the lifespan. Using multivariate PLS analysis, we found that all networks exhibited stable patterns of network specific structural covariance, and—with the exception of the visual network—a second, age-dependent pattern of structural covariance that mirrored developmental trends seen in the functional connectivity literature. The present results confirm the utility of structural covariance in defining neurocognitive networks, suggest that the developmental trajectory of structural covariance networks may reflect functional influences, and reveal both shared and network specific trajectories of structural covariance across the lifespan.

bioRxiv preprint doi: https://doi.org/10.1101/090233; this version posted November 29, 2016. The copyright holder for this preprint (which was not certified by peer review) is the author/funder, who has granted bioRxiv a license to display the preprint in perpetuity. It is made available under aCC-BY 4.0 International license.

Acknowledgements

This work was supported in part by an Alzheimer's Association grant (NIRG-14-320049) to R.N.S. **NIH Peds** data used in the preparation of this article were obtained from the NIH Pediatric MRI Data Repository created by the NIH MRI Study of Normal Brain Development. This is a multisite, longitudinal study of typically developing children from ages newborn through young adulthood conducted by the Brain Development Cooperative Group and supported by the National Institute of Child Health and Human Development, the National Institute on Drug Abuse, the National Institute of Mental Health, and the National Institute of Neurological Disorders and Stroke (Contract #s N01-HD02-3343, N01-MH9-0002, and N01-NS-9-2314, -2315, -2316, -2317, -2319 and -2320). A listing of the participating sites and a complete listing of the study investigators can be found at http://pediatricmri.nih.gov/nihpd/info/participating_centers.html. **HCP** data were provided by the Human Connectome Project, WU-Minn Consortium (Principal Investigators: David Van Essen and Kamil Ugurbil; 1U54MH091657) funded by the 16 NIH Institutes and Centers that support the NIH Blueprint for Neuroscience Research; and by the McDonnell Center for Systems Neuroscience at Washington University. **NKI** data were obtained from the Nathan Kline Institute – Rockland Sample, Release 5. Principal support for the enhanced NKI-RS project is provided by the NIMH BRAINS R01MH094639-01 (Principal Investigator: Michael Milham). Funding for key personnel also provided in part by the New York State Office of Mental Health and Research Foundation for Mental Hygiene. Funding for the decompression and augmentation of administrative and phenotypic protocols provided by a grant from the Child Mind Institute (1FDN2012-1). Additional personnel support provided by the Center for the Developing Brain at the Child Mind Institute, as well as NIMH R01MH081218, R01MH083246, and R21MH084126. Project support also provided by the NKI Center for Advanced Brain Imaging (CABI), the Brain Research Foundation, and the Stavros Niarchos Foundation. **OASIS** data were supported by the following grants: P50 AG05681, P01 AG03991, R01 AG021910, P50 MH071616, U24 RR021382, R01 MH56584. **ADNI** data used in preparation of this article were obtained from the Alzheimer's Disease Neuroimaging Initiative (ADNI) database (adni.loni.usc.edu). As such, the investigators within the ADNI contributed to the design and implementation of ADNI and/or provided data but did not participate in analysis or writing of this report. A complete listing of ADNI investigators can be found at: http://adni.loni.usc.edu/wp-content/uploads/how_to_apply/ADNI_Acknowledgement_List.pdf. Data collection and sharing for this project was funded by the Alzheimer's Disease Data collection and sharing for this project was funded by the Alzheimer's Disease Neuroimaging Initiative (ADNI) (National Institutes of Health Grant U01 AG024904) and DOD ADNI (Department of Defense award number W81XWH-12-2-0012). ADNI is funded by the National Institute on Aging, the National Institute of Biomedical Imaging and Bioengineering, and through generous contributions from the following: AbbVie, Alzheimer's Association; Alzheimer's Drug Discovery Foundation; Araclon Biotech; BioClinica, Inc.; Biogen; Bristol-Myers Squibb Company; CereSpir, Inc.; Eisai Inc.; Elan Pharmaceuticals, Inc.; Eli Lilly and Company; EuroImmun; F. Hoffmann-La Roche Ltd and its affiliated company Genentech, Inc.; Fujirebio; GE Healthcare; IXICO Ltd.; Janssen Alzheimer Immunotherapy Research & Development, LLC.; Johnson & Johnson

bioRxiv preprint doi: https://doi.org/10.1101/090233; this version posted November 29, 2016. The copyright holder for this preprint (which was not certified by peer review) is the author/funder, who has granted bioRxiv a license to display the preprint in perpetuity. It is made available under aCC-BY 4.0 International license.

Pharmaceutical Research & Development LLC.; Lumosity; Lundbeck; Merck & Co., Inc.; Meso Scale Diagnostics, LLC.; NeuroRx Research; Neurotrack Technologies; Novartis Pharmaceuticals Corporation; Pfizer Inc.; Piramal Imaging; Servier; Takeda Pharmaceutical Company; and Transition Therapeutics. The Canadian Institutes of Health Research is providing funds to support ADNI clinical sites in Canada. Private sector contributions are facilitated by the Foundation for the National Institutes of Health (www.fnih.org). The grantee organization is the Northern California Institute for Research and Education, and the study is coordinated by the Alzheimer's Disease Cooperative Study at the University of California, San Diego. ADNI data are disseminated by the Laboratory for Neuro Imaging at the University of Southern California. This manuscript reflects the views of the authors and may not reflect the opinions or views of the NIH.

bioRxiv preprint doi: https://doi.org/10.1101/090233; this version posted November 29, 2016. The copyright holder for this preprint (which was not certified by peer review) is the author/funder, who has granted bioRxiv a license to display the preprint in perpetuity. It is made available under aCC-BY 4.0 International license.

References

Alexander-Bloch, A., Clasen, L., Stockman, M., Ronan, L., Lalonde, F., Giedd, J., & Raznahan, A. (2016). Subtle in-scanner motion biases automated measurement of brain anatomy from in vivo MRI. *Human Brain Mapping*, *37*, 2385-2397.

Alexander-Bloch, A., Giedd, J.N., & Bullmore, E. (2013). Imaging structural co-variance between human brain regions. *Nature Reviews: Neuroscience*, *14*, 322–336.

Alexander-Bloch, A., Raznahan, A., Bullmore, E., & Giedd, J. (2013). The convergence of maturational change and structural covariance in human cortical networks. *Journal of Neuroscience*, *33*, 2889–2899.

Ashburner, J. (2007). A fast diffeomorphic registration algorithm. *NeuroImage*, *38*, 95-113.

Ashburner, J. & Friston, K.J. (2000). Voxel-based morphometry—the methods. *NeuroImage*, *11*, 805-821.

Bassett, D.S., Bullmore, E., Verchinski, B.A., Mattay, V.S., Weinberger, D.R., Meyer-Lindenberg, A. (2008). Hierarchical organization of human cortical networks in health and schizophrenia. *Journal of Neuroscience*, *28*, 9239-9248.

Betzel, R.F., Byrge, L., He, Y., Goñi, J., Zuo, X.N., & Sporns, O. (2014). Changes in structural and functional connectivity among resting-state networks across the human lifespan. *NeuroImage*, *102*, 345–357.

Brain Development Cooperative Group & Evans, A.C. (2007). The NIH MRI study of normal brain development. *NeuroImage*, *30*, 184-202.

Bullmore, E., & Sporns, O. (2009). Complex brain networks: graph theoretical analysis of structural and functional systems. *Nature Reviews: Neuroscience*, *10*, 186–198.

Caviness, V.S. Jr, Kennedy, D.N., Richelme, C., Rademacher J., & Filipek, P.A. (1996). The human brain age 7–11 years: a volumetric analysis based on magnetic resonance images. *Cerebral Cortex*, *6*, 726–736.

Chan, M.Y., Park, D.C., Savalia, N.K., Petersen, S.E., & Wig, G.S. (2014). Decreased segregation of brain systems across the healthy adult lifespan. *Proceedings of the National Academy of Sciences*, *111*, 4997-5006.

Chang, L.J., Yarkoni, T., Khaw, M.W., & Sanfey, A.G. (2013). Decoding the role of the insula in human cognition: Functional parcellation and large-scale reverse inference. *Cerebral Cortex*, *23*, 739-749.

Collin, G., & van den Heuvel, M.P. (2013). The ontogeny of the human connectome: Development and dynamic changes of brain connectivity across the life span. *Neuroscientist*, *19*, 616–28.

Cox, R.W. (1996). AFNI: Software for analysis and visualization of functional magnetic resonance neuroimages. *Computers and Biomedical Research*, *29*,162–173.

Craig, A.D. (2009). How do you feel—now? The anterior insula and human awareness. *Nature Reviews: Neuroscience*, *10*, 59-70.

bioRxiv preprint doi: https://doi.org/10.1101/090233; this version posted November 29, 2016. The copyright holder for this preprint (which was not certified by peer review) is the author/funder, who has granted bioRxiv a license to display the preprint in perpetuity. It is made available under aCC-BY 4.0 International license.

Dosenbach, N.U.F., Nardos, B., Cohen, A.L., Fair, D.A., Power, J.D., Church, J.A., … Schlaggar, B.L. (2010). Prediction of individual brain maturity using fMRI. *Science*, *329*, 1358–1361.

Eckart, C. & Young, G. (1936). The approximation of one matrix by another of lower rank. *Psychometrika*, *1*, 211–218.

Fjell, A.M., Westlye, L.T., Espeseth, T., Reinvang, I., Walhovd, K.B., Dale, A.M., & Holland, D. (2010). Cortical gray matter atrophy in healthy aging cannot be explained by undetected incipient cognitive disorders: A comment on Burgmans et al. (2009). *Neuropsychology*, *24*, 258-266.

Geerligs, L., Cam-CAN, & Henson, R.N. (2016). Functional connectivity and structural covariance between regions of interest can be measured more accurately using multivariate distance correlation. *NeuroImage*. Advance online publication. doi: 10.1016/j.neuroimage.2016.04.047

Geerligs, L., Renken, R.J., Saliasi, E., Maurits, N.M., Lorist, M.M. (2015). A brain-wide study of age-related changes in functional connectivity. *Cerebral Cortex*, *25*, 1987-1999.

Giorgio, A., Santelli, L., Tomassini, V., Bosnell, R., Smith, S., De Stefano, N., & Johansen-Berg, H. (2010). Age-related changes in grey and white matter structure throughout adulthood. *NeuroImage*, *51*, 943-951.

Glasser, M.F., Smith, S.M., Marcus, D.S., Andersson, J.L.R., Auerbach, E.J., Behrens, T.E.J., … Van Essen, D.C. (2016). The Human Connectome Project's neuroimaging approach. *Nature Neuroscience*, *19*, 1175-1187.

Hafkemeijer, A., Altmann-Schneider, I., de Craen, A.J.M., Slagboom, P.E., van der Grond, J., & Rombouts, S.A.R.B. (2014). Associations between age and gray matter volume in anatomical brain networks in middle-aged to older adults. *Aging Cell*, *13*, 1068-1074.

Hafkemeijer, A., Möller, C., Dopper, E.G.P., Jiskoot, L.C., van den Berg-Huysmans, A.A., van Swieten, J.C., … Rombouts, S.A.R.B. (2016). Differences in structural covariance networks between behavioral variant frontotemporal dementia and Alzheimer's disease. *Human Brain Mapping*, *37*, 978-988.

Hagmann, P., Sporns, O., Madan, N., Cammoun, L., Pienarr, R., Wedeen, V.J., ….Grant, P.E. (2010). White matter maturation reshapes structural connectivity in the late developing human brain. *Proceedings of the National Academy of Sciences*, *107*, 19067-19072.

Jilka, S.R., Scott, G., Ham, T., Pickering, A., Bonnelle, V., Braga, R.M., … Sharp, D.J. (2014). Damage to the salience network and interactions with the default mode network. *Journal of Neuroscience*, *34*, 10798-10807.

Krishnan, A., Williams, L.J., McIntosh, A.R., & Abdi, H. (2011). Partial Least Squares (PLS) methods for neuroimaging: a tutorial and review. *NeuroImage*, *56*, 455–75.

bioRxiv preprint doi: https://doi.org/10.1101/090233; this version posted November 29, 2016. The copyright holder for this preprint (which was not certified by peer review) is the author/funder, who has granted bioRxiv a license to display the preprint in perpetuity. It is made available under aCC-BY 4.0 International license.

Krongold, M., Cooper, C., & Bray, S. (2015). Modular development of cortical gray matter across childhood and adolescence. *Cerebral Cortex*. Advance online publication. doi:10.1093/cercor/bhv307

Low, L.K., & Cheng, H.-J. (2006). Axon pruning: an essential step underlying the developmental plasticity of neuronal connections. *Philosophical Transactions of the Royal Society B*, *361*, 1531–44.

McIntosh, A., Bookstein, F., Haxby, J., & Grady, C. (1996). Spatial pattern analysis of functional brain images using partial least squares. *NeuroImage*, *3*, 143–157.

Mechelli, A., Friston, K.J., Frackowiak, R.S., & Price, C.J. (2005) Structural covariance in the human cortex. *Journal of Neuroscience*, *25*, 8303–8310.

Mesulam, M.M. (1998). From sensation to cognition. *Brain*, *121*, 1013-1052.

Miller, K.L., Alfaro-Almagro, F., Bangerter, N.K., Thomas, D.L., Yacoub, E., Xu, J., … Smith, S.M. (2016). Multimodal population brain imaging in the UK Biobank prospective epidemiological study. *Nature Neuroscience*. Advance online publication. doi: 10.1038/nn.4393

Mišić, B., Betzel, R.F., de Reus, M.A., van den Heuvel, M.P., Berman, M.G., McIntosh, A.R., & Sporns, O. (2016). Network-level structure-function relationships in human neocortex. *Cerebral Cortex*. Advance online publication. doi: 10.1093/cercor/bhw089

Montembeault, M., Joubert, S., Doyon, J., Carrier, J., Gagnon, J. F., Monchi, O., … Brambati, S. M. (2012). The impact of aging on gray matter structural covariance networks. *NeuroImage*, *63*, 754–759.

Muzik, O., Chugani, D.C., Juhasz, C., Shen, C.G., & Chugani, H.T. (2000). Statistical parametric mapping: Assessment of application in children. *NeuroImage*, *12*, 538–549.

Nooner, K.B., Colcombe, S.J., Tobe, R.H., Mennes, M., Benedict, M.M., Moreno, A.L., … Milham, M.P. (2012). The NKI-Rockland sample: A model for accelerating the pace of discovery science in psychiatry. *Frontiers in Neuroscience*, *6*. doi: 10.3389/fnins.2012.00152.

Pagani, M., Bifone, A., & Gozzi, A. (2016). Structural covariance networks in the mouse brain. *NeuroImage*, *129*, 55-63.

Persson, J., Spreng, R.N., Turner, G., Herlitz, A., Morell, A., Stening, E., … Söderlund, H. (2014). Sex differences in volume and structural covariance of the anterior and posterior hippocampus. *NeuroImage*, 99, 215-225.

Power, J.D., Cohen, A.L., Nelson, S.M., Wig, G.S., Barnes, K.A., Church, J.A., … Petersen, S.E. (2011). Functional network organization of the human brain. *Neuron*, *72*, 665–678.

Raz, N., Lindenberger, U., Rodrigue, K.M., Kennedy, K.M., Head, D., Williamson, A., … Acker, J.D. (2005). Regional brain changes in aging healthy adults: General trends, individual differences and modifiers. *Cerebral Cortex*, *15*, 1676–1689.

bioRxiv preprint doi: https://doi.org/10.1101/090233; this version posted November 29, 2016. The copyright holder for this preprint (which was not certified by peer review) is the author/funder, who has granted bioRxiv a license to display the preprint in perpetuity. It is made available under aCC-BY 4.0 International license.

Savalia, N.K., Agres, P.F., Chan, M.Y., Feczko, E.J., Kennedy, K.M., Wig, G.S. (2016). Motion-related artifacts in structural brain images revealed with independent estimates of in-scanner head motion. *Human Brain Mapping*. Advance online publication. doi: 10.1002/hbm.23397

Seeley, W.W., Crawford, R.K., Zhou, J., Miller, B.L., & Grecius, M.D. (2009). Neurodegenerative diseases target large-scale human brain networks. *Neuron*, *62*, 42-52.

Spreng, R.N., & Turner, G.R. (2013). Structural covariance of the default network in healthy and pathological aging. *Journal of Neuroscience*, *33*, 15226-15234.

Stevens, W.D., & Spreng, R.N. (2014). Resting-state functional connectivity MRI reveals active processes central to cognition. *Wiley Interdisciplinary Reviews: Cognitive Science*, *5*, 233–245.

Sui, J., Huster, R., Yu, Q., Segall, J.M., & Calhoun, V.D. (2014). Function-structure associations of the brain: Evidence from multimodal connectivity and covariance studies. *NeuroImage*, *102*, 11-23.

Tijms, B.M., Seris, P., Willshaw, D.J., & Lawrie, S.M. (2012). Similarity-based extraction of individual networks from gray matter MRI scans. *Cerebral Cortex*, *22*, 1530–1541.

Valk, S.L., Martino, A.D., Milham, M.P., & Bernhardt, B.C. (2015). Multicenter mapping of structural network alterations in autism. *Human Brain Mapping*, *36*, 2364-2373.

van den Heuvel, M.P., & Sporns, O. (2013). Network hubs in the human brain. *Trends in Cognitive Neurosciences*, *17*, 683-696.

Yeo, B.T.T., Krienen, F.M., Sepulcre, J., Sabuncu, M.R., Lashkari, D., Hollinshead, M., … Buckner, R.L. (2011). The organization of the human cerebral cortex estimated by intrinsic functional connectivity. *Journal of Neurophysiology*, *106*, 1125–65.

Zielinski, B.A., Gennatas, E.D., Zhou, J., & Seeley, W.W. (2010). Network-level structural covariance in the developing brain. *Proceedings of the National Academy of Sciences*, *107*, 18191–18196.

Zuo, X.-N., He, Y., Betzel, R. F., Colcombe, S., Sporns, O., & Milham, M. P. (2016). Human Connectomics across the Life Span. *Trends in Cognitive Sciences*, Advance online publication. doi: 10.1016/j.tics.2016.10.005

Table 1
Image Acquisition Parameters by Data Source.

	Scanner Strength (T)	TR (ms)	TE (ms)	TI (ms)	TD (ms)	Flip Angle (deg.)	FOV (mm)	Voxel Size (mm)
NIH-Peds	1.5	22-25	10-11				256×160-180	1.0 × 1.0 × 1.0-1.5
HCP	3	2400	2.14	1000	0	8	224×224	0.7 × 0.7 × 0.7
NKI-RS	3	1900	2.52	900	0	9	250×250	1.0 × 1.0 × 1.0
OASIS	1.5	9.7	4.0	20	200	10	256×256	1.0 × 1.0 × 1.25
ADNI	1.5	2400	min. full	1000	0	8	240×240	0.94 × 0.94 ×1.2

Table 2

Participant Characteristics by Age Group.

Age Group	Sample Size (Males)	Age in Years *M* (*SD*)	Scanned at 1.5T/3T
6-15y	330 (159)	10 (2.66)	306/24
16-25y	302 (139)	21 (2.8)	176/126
26-35y	472 (192)	30 (2.74)	31/441
36-59y	139 (38)	49 (6.29)	68/71
60-75y	203 (82)	70 (4.16)	157/46
76-94y	134 (49)	81 (4.28)	121/13

bioRxiv preprint doi: https://doi.org/10.1101/090233; this version posted November 29, 2016. The copyright holder for this preprint (which was not certified by peer review) is the author/funder, who has granted bioRxiv a license to display the preprint in perpetuity. It is made available under aCC-BY 4.0 International license.

Table 3

Selected Seeds for Each Network.

Network Affiliation	*x*	*y*	*z*	Laterality	Anatomical Label
Default	-7	49	18	L	Medial Prefrontal Cortex
	-7	-52	26	L	Posterior Cingulate Cortex
	-41	-60	29	L	Inferior Parietal Lobule
	41	-60	29	R	Inferior Parietal Lobule
Dorsal Attention	-22	-8	54	L	Frontal Eye Fields
	22	-8	54	R	Frontal Eye Fields
	-51	-64	-2	L	Middle Temporal Motion Complex
	51	-64	-2	R	Middle Temporal Motion Complex
Frontoparietal Control	-40	50	7	L	Frontal Pole
	40	50	7	R	Frontal Pole
	-43	-50	46	L	Anterior Inferior Parietal Lobule
	43	-50	46	R	Anterior Inferior Parietal Lobule
Ventral Attention	-5	15	32	L	Anterior Cingulate Cortex
	5	15	32	R	Anterior Cingulate Cortex
	-31	11	8	L	Anterior Insula
	31	11	8	R	Anterior Insula
Somatomotor	-41	-20	62	L	Precentral Gyrus (Hand)
	41	-20	62	R	Precentral Gyrus (Hand)
	-55	-4	26	L	Precentral Gyrus (Tongue)
	55	-4	26	R	Precentral Gyrus (Tongue)
Visual	-3	-74	23	L	Extrastriate Visual Cortex
	3	-74	23	R	Extrastriate Visual Cortex
	-16	-74	7	L	Visual Area 1
	16	-74	7	R	Visual Area 1

Coordinates (*x*, *y*, *z*) are in MNI stereotaxic space.

bioRxiv preprint doi: https://doi.org/10.1101/090233; this version posted November 29, 2016. The copyright holder for this preprint (which was not certified by peer review) is the author/funder, who has granted bioRxiv a license to display the preprint in perpetuity. It is made available under aCC-BY 4.0 International license.

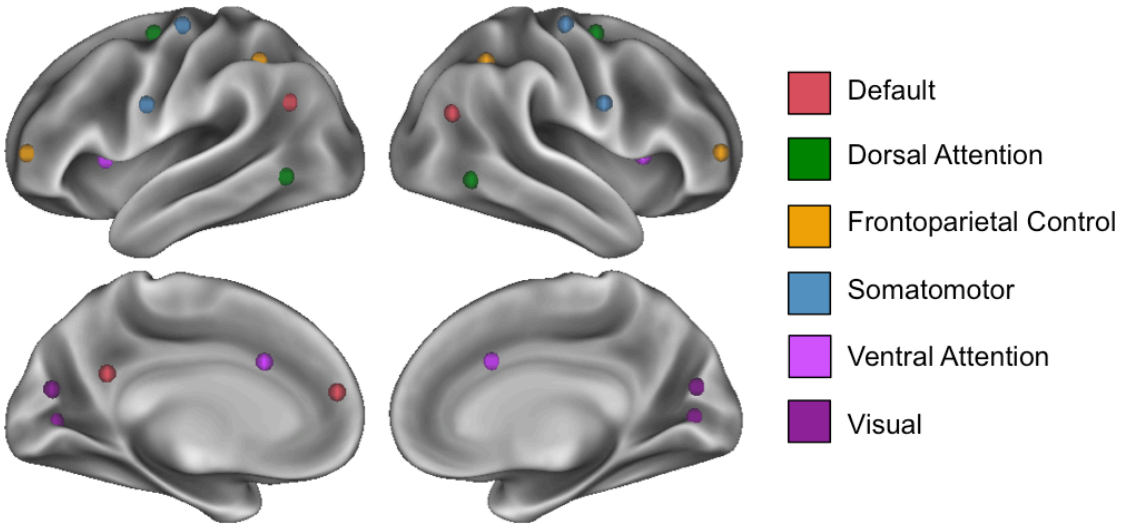

Figure 1. Selected seeded regions. The four selected seeded regions for each of the six neurocognitive networks are depicted in colors corresponding to their Yeo and colleagues (2011) labeling.

bioRxiv preprint doi: https://doi.org/10.1101/090233; this version posted November 29, 2016. The copyright holder for this preprint (which was not certified by peer review) is the author/funder, who has granted bioRxiv a license to display the preprint in perpetuity. It is made available under aCC-BY 4.0 International license.

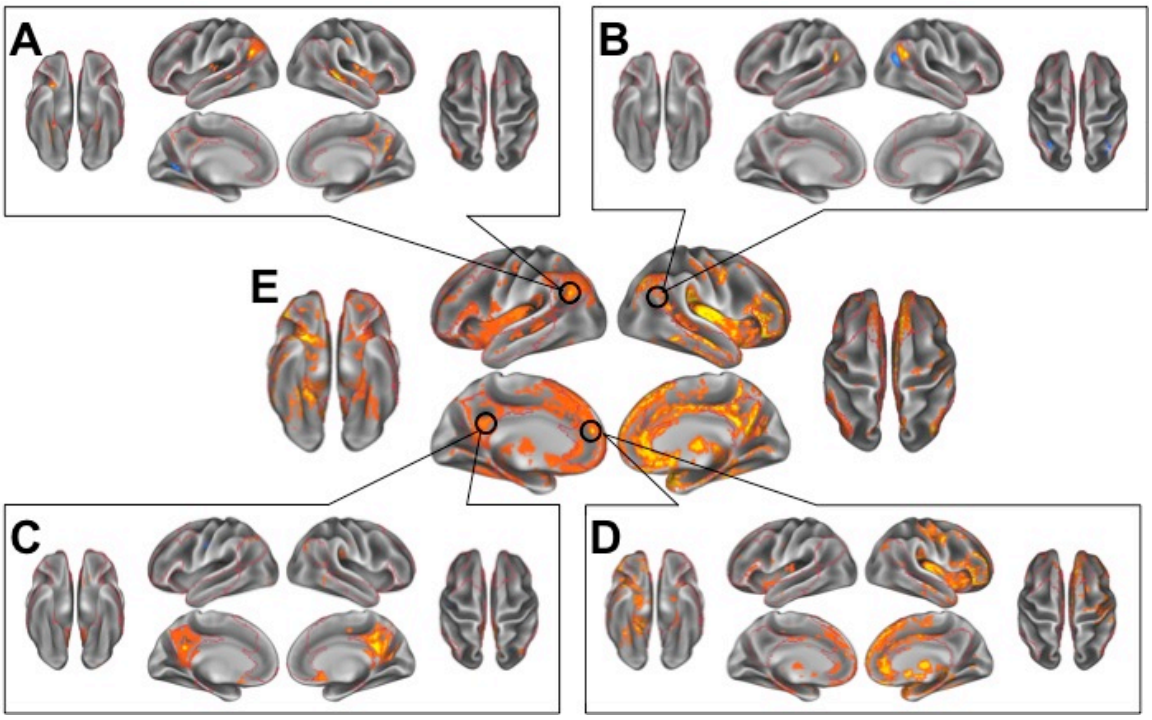

Figure 2. Impact of seed selection in network definition. Structural covariance patterns of the default network in the young adult cohort derived by differential seed selection. (A) Structural covariance of the left inferior parietal lobule seed. (B) Structural covariance of the right inferior parietal lobule seed. (C) Structural covariance of the posterior cingulate cortex seed. (D) Structural covariance of the medial prefrontal cortex seed. (E) Structural covariance of all four seeds entered individually, rather than averaged.

bioRxiv preprint doi: https://doi.org/10.1101/090233; this version posted November 29, 2016. The copyright holder for this preprint (which was not certified by peer review) is the author/funder, who has granted bioRxiv a license to display the preprint in perpetuity. It is made available under aCC-BY 4.0 International license.

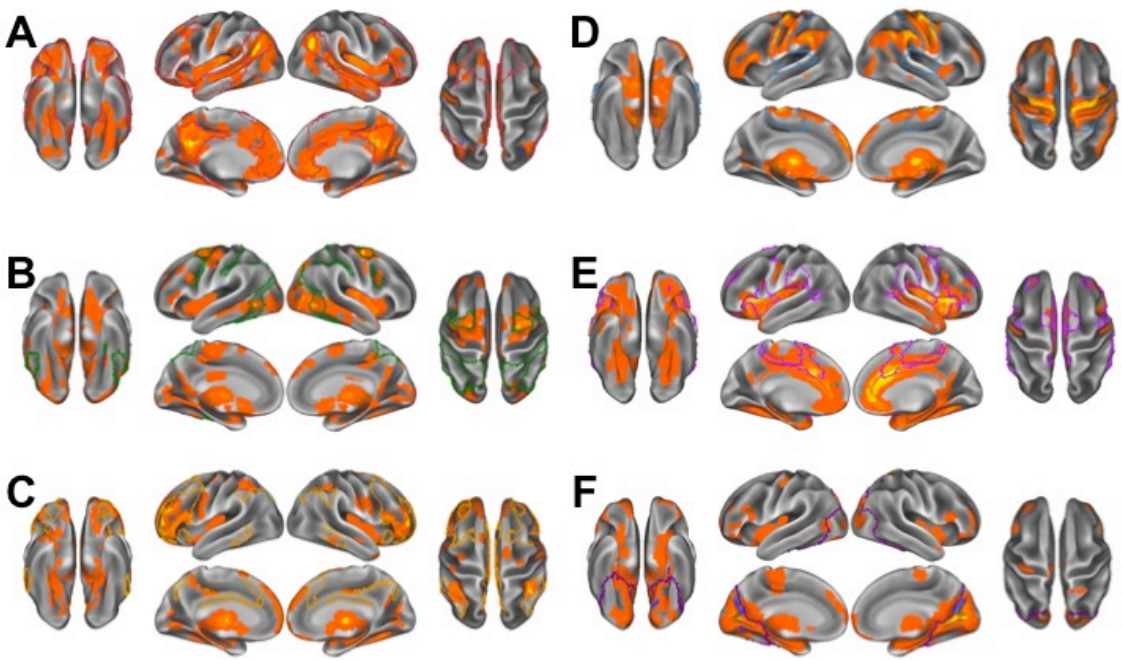

Figure 3. Comparing structural covariance and functional parcellations. Structural covariance patterns of each of the six neurocognitive networks in the young adult age group. Overlaid are their respective resting-state functional connectivity parcellation from Yeo and colleagues (2011). (A) The default network. (B) The dorsal attention network. (C) The frontoparietal control network. (D) The somatomotor network. (E) The ventral attention network. (F) The visual network.

bioRxiv preprint doi: https://doi.org/10.1101/090233; this version posted November 29, 2016. The copyright holder for this preprint (which was not certified by peer review) is the author/funder, who has granted bioRxiv a license to display the preprint in perpetuity. It is made available under aCC-BY 4.0 International license.

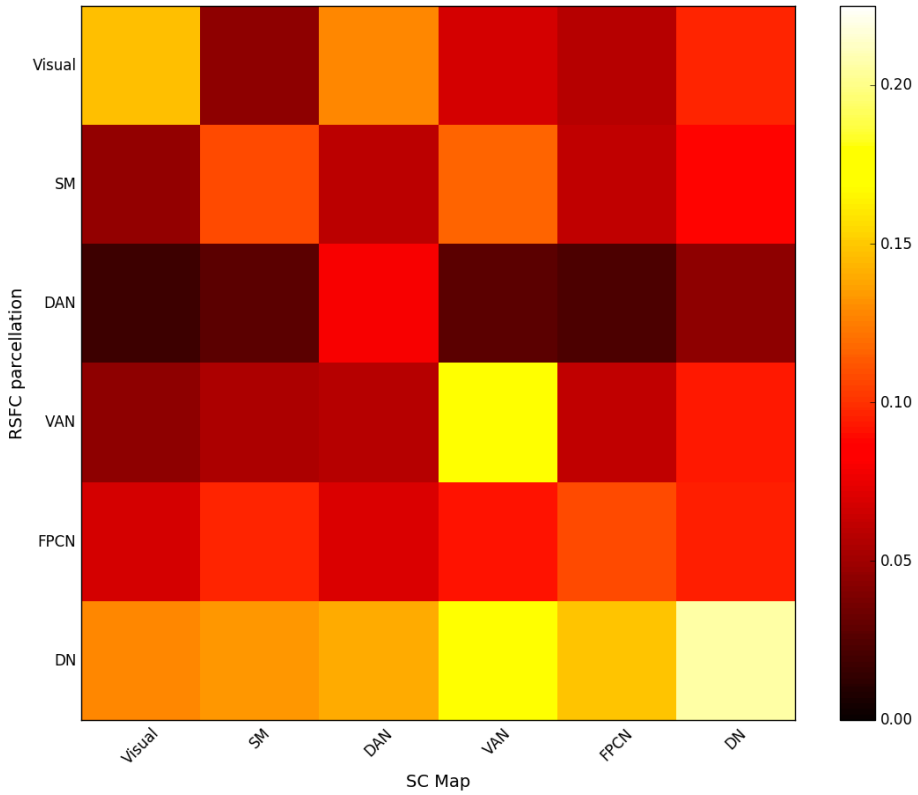

Figure 4. Heat map of dice similarity values. A heat map of dice similarity values between resting-state functional connectivity parcellation and structural covariance map for each of the six neurocognitive networks. Warmer colors indicate higher similarity. DN: Default Network. DAN: Dorsal Attention Network. FPCN: Frontoparietal Control Network. RSFC: Resting State Functional Connectivity. SC: Structural Covariance. SM: Somatomotor Network. VAN: Ventral Attention Network. Visual: Visual Network.

bioRxiv preprint doi: https://doi.org/10.1101/090233; this version posted November 29, 2016. The copyright holder for this preprint (which was not certified by peer review) is the author/funder, who has granted bioRxiv a license to display the preprint in perpetuity. It is made available under aCC-BY 4.0 International license.

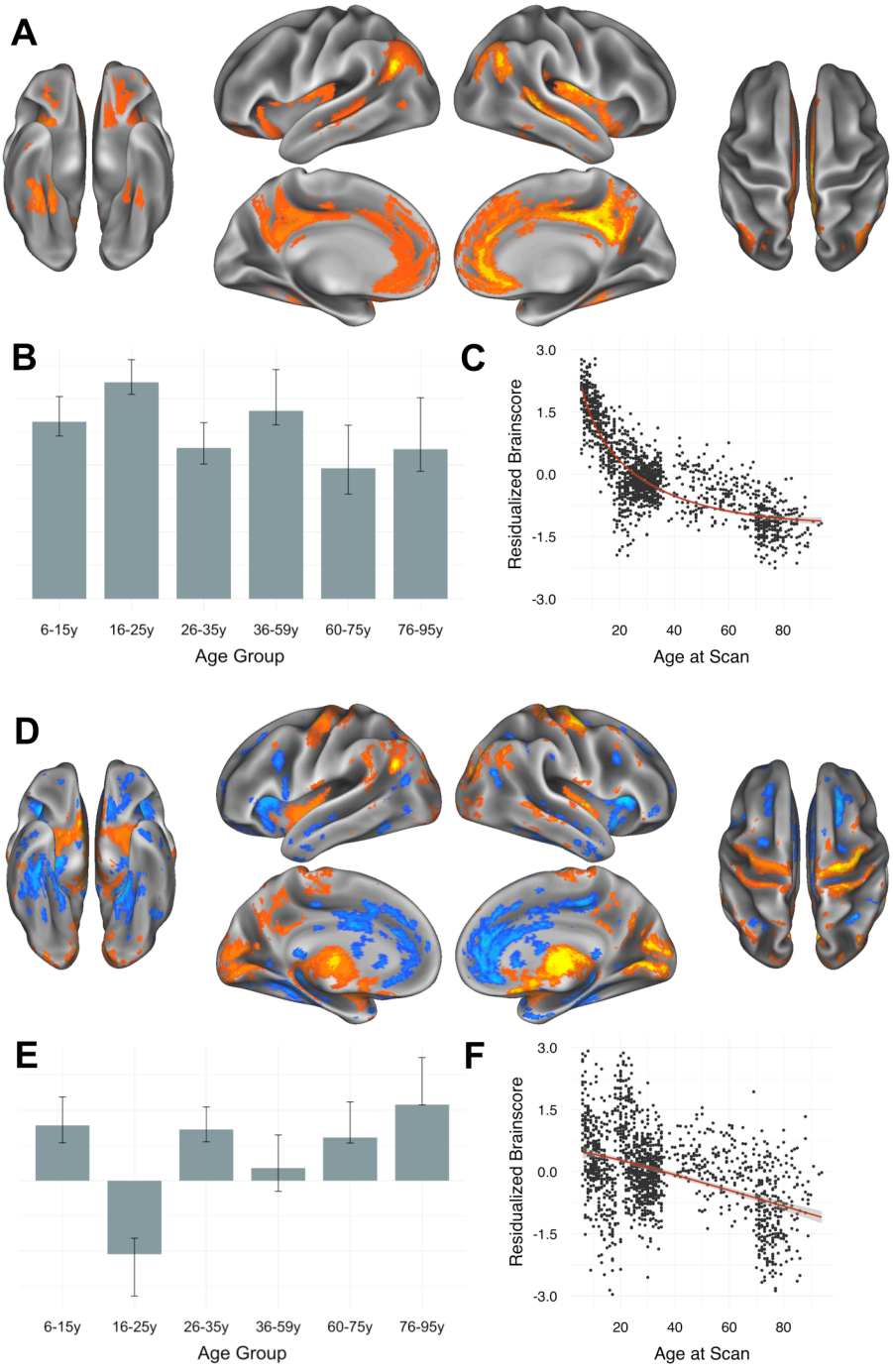

Figure 5. Structural covariance of the default network. Derived structural covariance patterns of the default network. (A) The spatial pattern for the first latent variable. (B) The averaged brain scores by age group for the first latent variable. (C) The individual brain scores. (D), (E), and (F) depict these results for the second latent variable.

bioRxiv preprint doi: https://doi.org/10.1101/090233; this version posted November 29, 2016. The copyright holder for this preprint (which was not certified by peer review) is the author/funder, who has granted bioRxiv a license to display the preprint in perpetuity. It is made available under aCC-BY 4.0 International license.

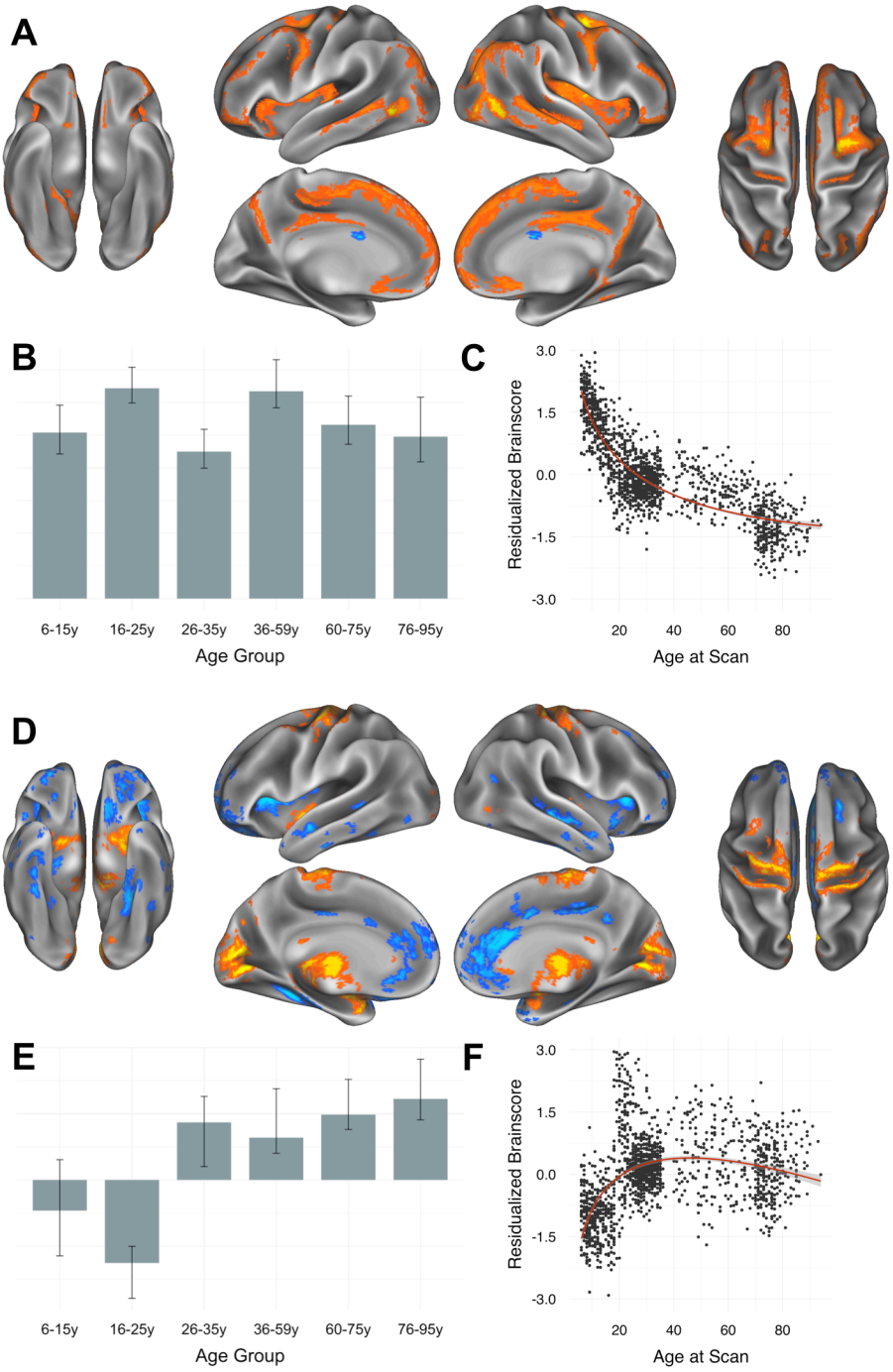

Figure 6. Structural covariance of the dorsal attention network. Derived structural covariance patterns of the dorsal attention network. (A) The spatial pattern for the first latent variable. (B) The averaged brain scores by age group for the first latent variable. (C) The individual brain scores. (D), (E), and (F) depict these results for the second latent variable.

bioRxiv preprint doi: https://doi.org/10.1101/090233; this version posted November 29, 2016. The copyright holder for this preprint (which was not certified by peer review) is the author/funder, who has granted bioRxiv a license to display the preprint in perpetuity. It is made available under aCC-BY 4.0 International license.

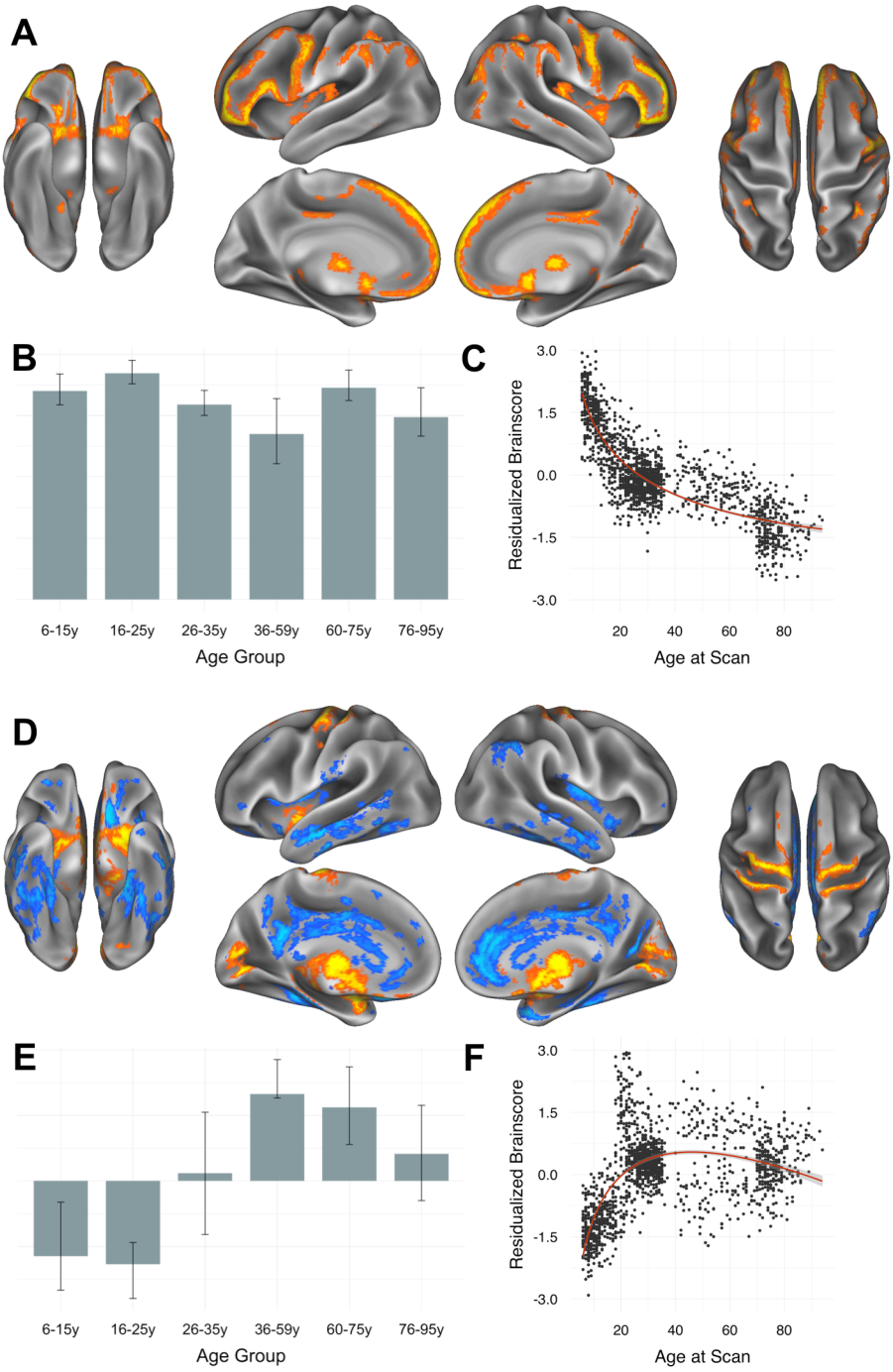

Figure 7. Structural covariance of the frontoparietal control network. Derived structural covariance patterns of the frontoparietal control network. (A) The spatial pattern for the first latent variable. (B) The averaged brain scores by age group for the first latent variable. (C) The individual brain scores. (D), (E), and (F) depict these results for the second latent variable.

bioRxiv preprint doi: https://doi.org/10.1101/090233; this version posted November 29, 2016. The copyright holder for this preprint (which was not certified by peer review) is the author/funder, who has granted bioRxiv a license to display the preprint in perpetuity. It is made available under aCC-BY 4.0 International license.

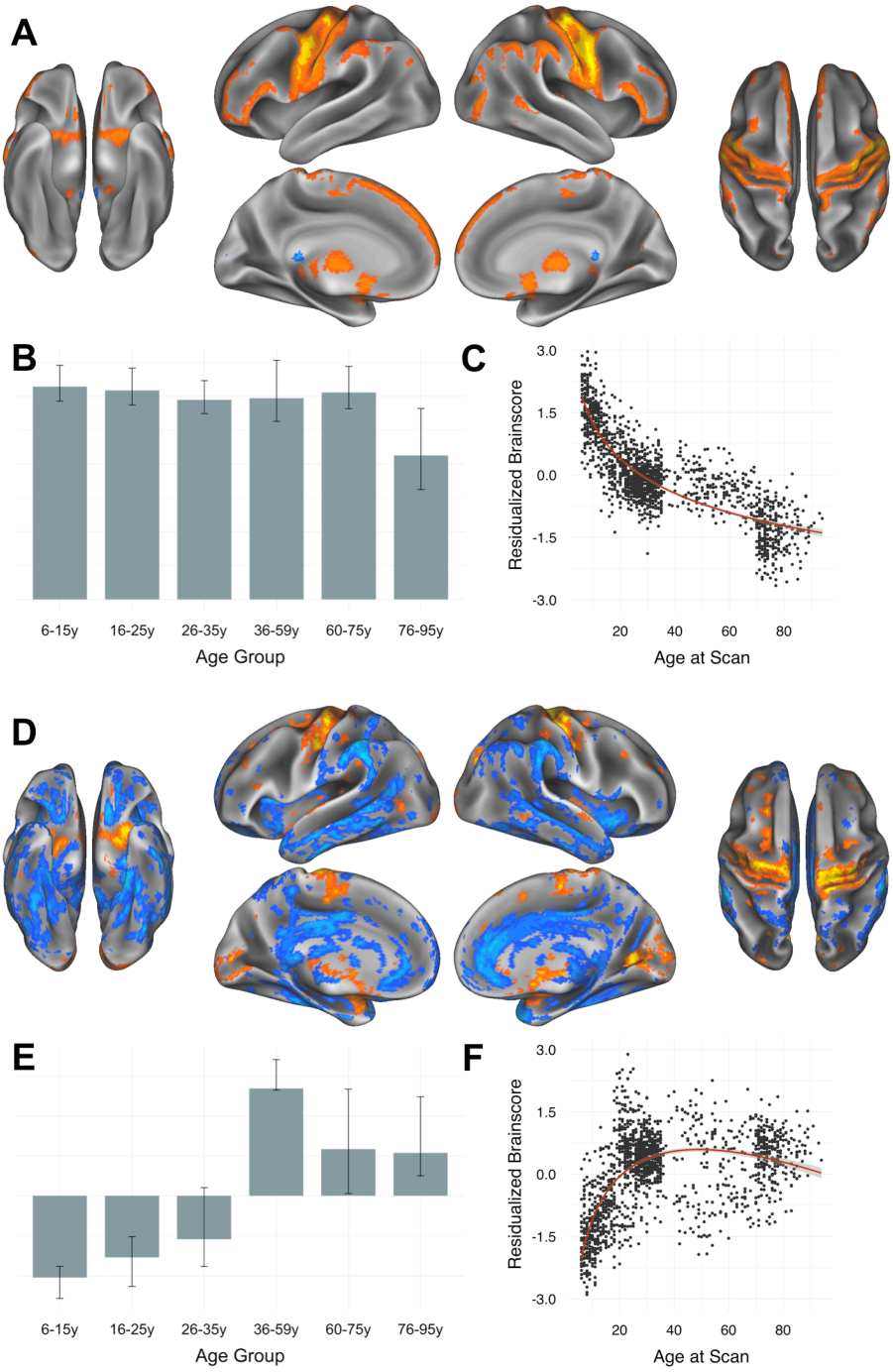

Figure 8. Structural covariance of the somatomotor network. Derived structural covariance patterns of the somatomotor network. (A) The spatial pattern for the first latent variable. (B) The averaged brain scores by age group for the first latent variable. (C) The individual brain scores. (D), (E), and (F) depict these results for the second latent variable.

bioRxiv preprint doi: https://doi.org/10.1101/090233; this version posted November 29, 2016. The copyright holder for this preprint (which was not certified by peer review) is the author/funder, who has granted bioRxiv a license to display the preprint in perpetuity. It is made available under aCC-BY 4.0 International license.

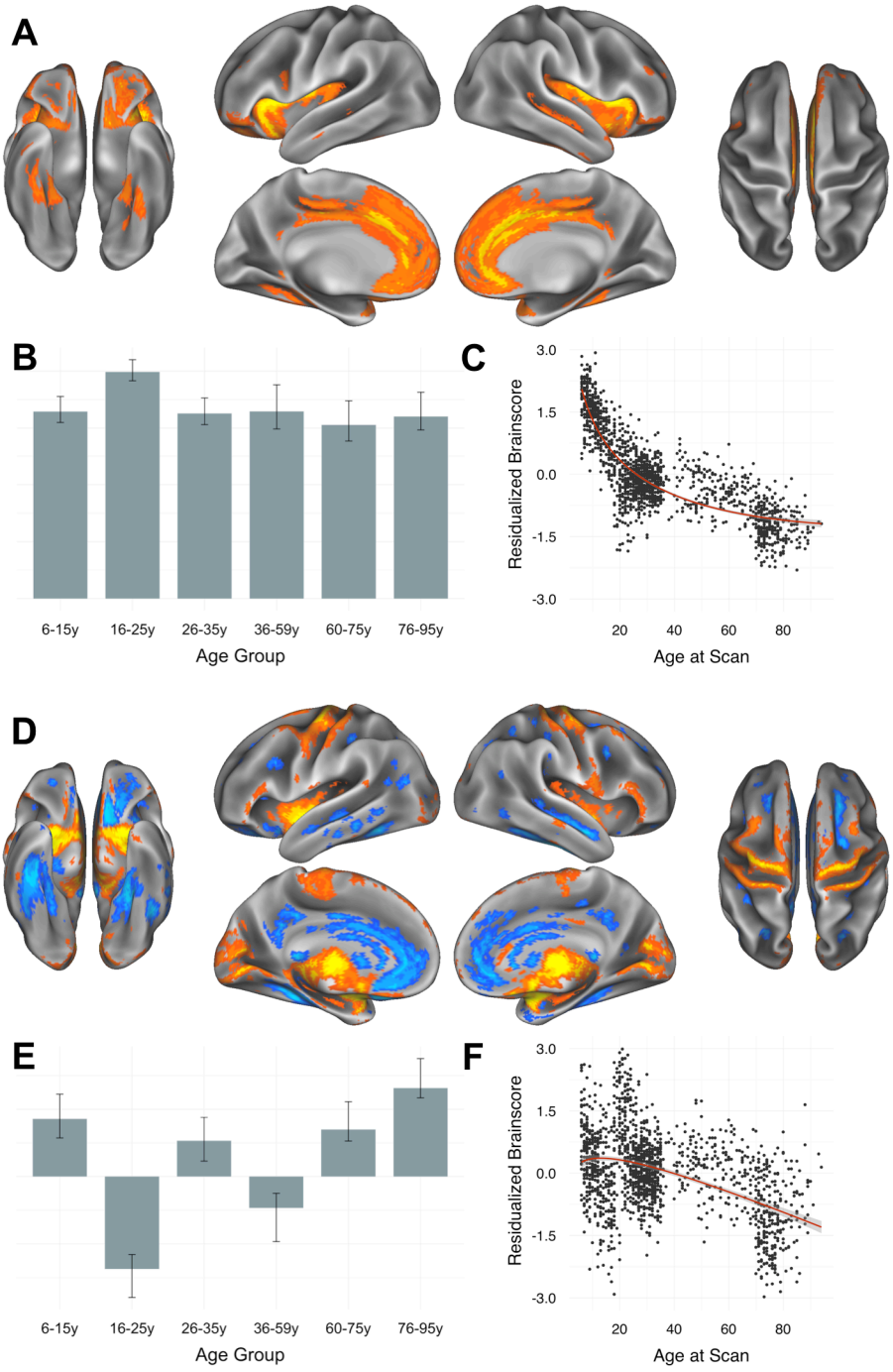

Figure 9. Structural covariance of the ventral attention network. Derived structural covariance patterns of the ventral attention network. (A) The spatial pattern for the first latent variable. (B) The averaged brain scores by age group for the first latent variable. (C) The individual brain scores. (D), (E), and (F) depict these results for the second latent variable.

bioRxiv preprint doi: https://doi.org/10.1101/090233; this version posted November 29, 2016. The copyright holder for this preprint (which was not certified by peer review) is the author/funder, who has granted bioRxiv a license to display the preprint in perpetuity. It is made available under aCC-BY 4.0 International license.

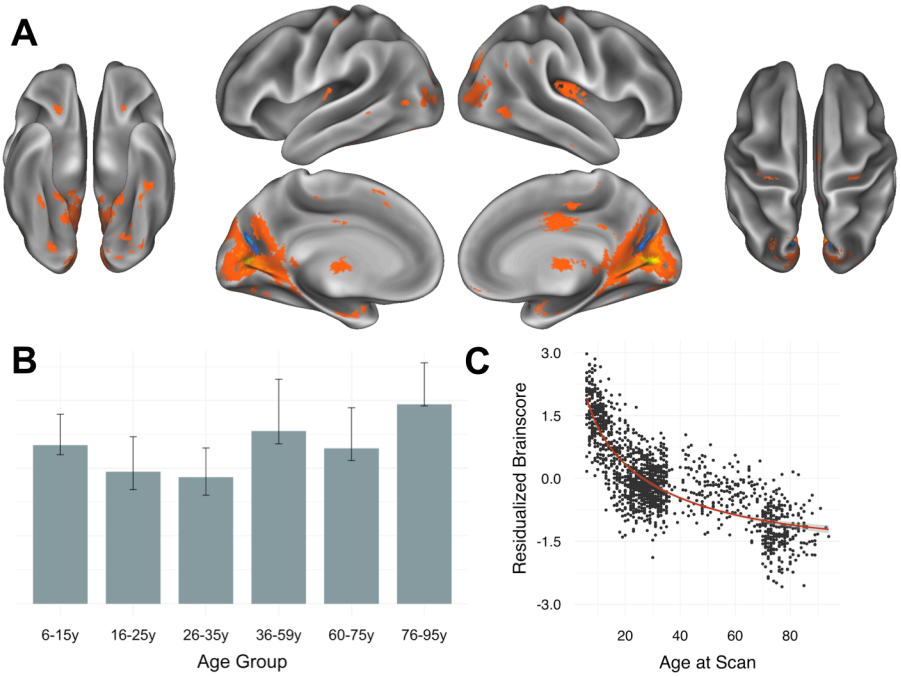

Figure 10. Structural covariance of the visual network. Derived structural covariance patterns of the visual network. (A) The spatial pattern for the first latent variable. (B) The averaged brain scores by age group for the first latent variable. (C) The individual brain scores.